

# Geophysical Research Letters

## RESEARCH LETTER

10.1029/2019GL082548

### Key Points:

- We have performed the first plasma simulations of the interaction of the Moon's ancient dynamo field and the solar wind
- Dynamo fields of 0.5–5  $\mu\text{T}$  decrease the global solar wind  $\text{H}^+$  surface flux by 60–90%; polar region flux increases by nearly tenfold
- These changes in global and polar fluxes of  $\text{H}^+$  may influence the rates of accumulation and weathering of polar volatile deposits

### Correspondence to:

I. Garrick-Bethell,  
igarrick@ucsc.edu

### Citation:




Garrick-Bethell, I., Poppe, A. R., & Fatemi, S. (2019). The lunar paleo-magnetosphere: implications for the accumulation of polar volatile deposits. *Geophysical Research Letters*, *46*. <https://doi.org/10.1029/2019GL082548>

Received 22 FEB 2019

Accepted 13 APR 2019

Accepted article online 17 APR 2019

## The Lunar Paleo-Magnetosphere: Implications for the Accumulation of Polar Volatile Deposits

I. Garrick-Bethell<sup>1,2</sup> , A. R. Poppe<sup>3,4</sup> , and S. Fatemi<sup>5</sup> 

<sup>1</sup>Department of Earth and Planetary Sciences, University of California, Santa Cruz, CA, USA, <sup>2</sup>School of Space Research, Kyung Hee University, Yongin-si, South Korea, <sup>3</sup>Space Sciences Laboratory, University of California, Berkeley, CA, USA, <sup>4</sup>Solar System Exploration Research Virtual Institute, NASA Ames Research Center, Mountain View, CA, USA, <sup>5</sup>Swedish Institute of Space Physics, Kiruna, Sweden

**Abstract** Analyses of lunar samples suggest the Moon once possessed a dynamo from ~4.25 Ga until perhaps as recently as 1 Ga, with surface field strengths between ~5 and 100  $\mu\text{T}$ . While the exact timing, strength, and structure of these paleomagnetic fields are not precisely known, such relatively strong fields imply that the Moon also likely possessed a magnetosphere. Here, we present hybrid plasma simulations of the structure and morphology of the putative lunar “paleo-magnetosphere” for varying surface field strengths and orientations, using ambient solar wind conditions representative of the early Sun. The presence of the paleo-magnetosphere reduces total solar wind fluxes to the lunar surface overall yet, for a spin-aligned dynamo, increases the relative solar wind flux to the lunar polar regions. In turn, the paleo-magnetosphere may have altered the rate of volatile accretion to the Moon over its history.

**Plain Language Summary** While the Moon currently does not possess a global magnetic field like the Earth, analyses of lunar rocks suggest that the Moon did possess a global magnetic field between 1 and 4.25 billion years ago. The field is estimated to be ~10% to 100% of the strength of Earth's present-day magnetic field. Such relatively strong magnetic fields at the Moon will form a magnetosphere, or a region of space surrounding the Moon where lunar magnetic fields dominate over the plasma and magnetic fields of the solar wind (a stream of charged particles emanating from the Sun). We use computer simulations to model the lunar paleo-magnetosphere with different field strengths and calculate the rate at which solar wind ions can still access the surface. The paleo-magnetosphere reduces the solar wind precipitation rate overall but focuses particles into the poles if the magnetic field is aligned with the Moon's spin axis.

### 1. Introduction

Several decades of lunar sample analysis and remote sensing studies have established that the Moon once possessed a dynamo (Fuller & Cisowski, 1987; Weiss & Tikoo, 2014). This dynamo may have existed from ~4.25 Ga to perhaps as recently as 1.0 Ga, with paleofields ranging from ~5 to 100  $\mu\text{T}$  at the surface (Garrick-Bethell et al., 2017; Tikoo et al., 2017). To date, there has been no analysis of how this dynamo field would have interacted with the early solar wind. On Ganymede and Mercury, dynamo fields block incident plasma access to parts of the surface under certain conditions (Cooper et al., 2001; Domingue et al., 2014; Fatemi et al., 2016; Poppe, Fatemi, et al. 2018). Similarly, it is likely that there was once significant magnetospheric shielding of solar wind access to the lunar surface, given that lunar surface paleofields were possibly 10 to 100 times higher than at present-day Mercury.

Unlike Ganymede and Mercury, it may be possible to assess the history of the Moon's “paleo-magnetosphere” through isotopes measured in ancient lunar soils returned by the Apollo program. Such isotopic records (Bogard et al., 1973; Eberhardt, 1972) have been used to constrain the evolution of the Sun's composition (Wieler, 2016) and the Moon's geologic history (Joy et al., 2011). The lunar dynamo field may have blocked implantation of lighter atomic ions and, at a minimum, reduced the implantation flux and energy of heavier ions. There are at least four important implications of this “magnetospheric fractionation” effect: (1) Proposed changes in the ratios of certain isotopes in the Sun over billions of years should be reassessed; (2) the strength of the early lunar field, which is not well constrained in all points in lunar history (Weiss & Tikoo, 2014), can be estimated, and the mere presence of some implanted species may indicate whether a field existed or not; (3) the accuracy of the antiquity indicator  $^{36}\text{Ar}/^{40}\text{Ar}$ , which makes use of solar wind  $^{36}\text{Ar}$  and indigenous  $^{40}\text{Ar}$  (Eugster et al., 2001), may need to be reassessed, or alternatively, the ratio

could also be used to estimate paleofield strength; and (4) production of OH and H<sub>2</sub>O through H implantation in regolith silicates may be arrested in the presence of a magnetic field, thereby reducing global-scale OH production (Pieters et al., 2009; Sunshine et al., 2009) and possible volatile migration to the paleopoles (Crider & Vondrak, 2002).

The interaction between the Moon's paleofield and the solar wind may also have implications for lunar paleomagnetism studies. For example, if the paleofield was weak enough, compressions of the magnetopause to the lunar surface under high solar wind pressure conditions could distort the local magnetic field at the lunar surface. This could confound efforts to infer the dynamo field orientation from Apollo samples (Cournède et al., 2012) and crustal magnetic anomalies (Nayak et al., 2017). The frequency and efficiency of such compression events may have been larger if the ancient solar wind density was higher than it is today (Airapetian & Usmanov, 2016) and if the sun produced more frequent coronal mass ejections (Airapetian et al., 2014). Such compressions could also enhance the surface field strength (Garrick-Bethell et al., 2018), possibly helping to explain the high inferred paleointensities of some Apollo samples beyond what can be explained by dynamo theory (Evans et al., 2018).

Here, we present the first simulations of the interaction of the dynamo field with the solar wind. The focus of this first study is to assess how the paleo-magnetosphere may have affected lunar surface water production by blocking of solar wind H<sup>+</sup> flux to the surface. The other magnetospheric effects discussed above will be investigated at a later time. At present, we do not model the interaction of the lunar dynamo field with plasmas in the terrestrial magnetotail, since the Moon spends only ~25% of its time in the magnetotail and a majority of the particle flux to the Moon originates from the solar wind (Poppe, Farrell, et al. 2018). The poles of the Moon have accumulated hydrogen (Colaprete et al., 2010; Feldman et al., 2001), but it is unknown if it is related to the solar wind (e.g., Crider & Vondrak, 2000), water liberated from micrometeoroid impacts (Füri et al., 2012), or some combination of both. If most of the Moon was shielded from H<sup>+</sup> implantation due to a dynamo field, solar wind water production and polar accumulation could have been arrested. In contrast, if the ancient dynamo drove solar wind particles to precipitate into polar regions, the local weathering rates of any exposed ices could have been enhanced, as suggested for Mercury (Delitsky et al., 2017). To investigate and potentially elucidate some of these competing effects, we have simulated two dynamo field geometries (dipoles perpendicular and parallel to the lunar spin axis) and three different equatorial surface field strengths (0.5, 2, and 5  $\mu$ T). Apollo samples were collected at low latitudes, and given the modest estimated amounts of true polar wander (Garrick-Bethell et al., 2014; Siegler et al., 2016), we assume for simplicity that the paleofields they recorded represent approximately paleo-equatorial fields. We use a three-dimensional plasma hybrid model (Fatemi et al., 2017) to model the lunar paleo-magnetosphere under assumed early solar system solar wind conditions. We use the results of the hybrid model to quantify the precipitation of solar wind H<sup>+</sup> to the lunar surface and compare our results to the unmagnetized case. Ultimately, we show that even the weakest expected dynamo fields can shield the surface from solar wind H<sup>+</sup> implantation relative to an unmagnetized case.

## 2. Model Description

We have used the Amitis hybrid plasma model (Fatemi et al., 2017) to investigate the solar wind interaction of the ancient lunar dynamo field with the early solar wind. Amitis employs the standard hybrid modeling technique by following individual ions according to particle-in-cell methods with electrons modeled as a charge-neutralizing fluid. Amitis has been extensively tested against standard metrics as reported in Fatemi et al. (2017) and was recently used to investigate the interaction between the present-day solar wind and, for example, the potentially magnetized asteroid 16 Psyche (Fatemi & Poppe, 2018) and Mercury (Fatemi et al., 2018). Here, the Moon is modeled as a purely resistive object that absorbs all particles that impact its surface; we neglect any possible effects from interior conductivity and associated induced fields (Dyal & Parkin, 1971; Fatemi et al., 2015; Sonett et al., 1971). We also neglect the possible production of plasma from planetary species (e.g., the role that Na<sup>+</sup> plays at Mercury with respect to nonadiabatic ion behavior, the introduction of additional plasma pressure terms, and the modification of Kelvin-Helmholtz waves; Gershman et al., 2015; Raines et al., 2015; Raines et al., 2011; Zurbuchen et al., 2011); however, we do note that the behavior of lunar ions within the paleo-magnetosphere (e.g., outgassed and ionized <sup>40</sup>Ar<sup>+</sup>) is of significant interest and identified as future research. All hybrid simulations are run

to steady state before saving the results (magnetic field, electric field, and particle distributions) for subsequent analysis.

The solar wind is believed to have changed considerably over time as the Sun evolved from birth to its present-day state. Observations of other stars have shown that stellar mass-loss rates and, by extension, stellar wind fluxes generally decrease with a star's age (Wood et al., 2005). Thus, in order to correctly model the possible lunar paleo-magnetosphere at  $\sim 2$  Gyr, one must select solar wind parameters representative of the desired epoch. Here, we employ the modeling results of Airapetian and Usmanov (2016) to quantify, at least to first-order, typical solar wind parameters at a solar age of  $\sim 2$  Gyr. In particular, Airapetian and Usmanov (2016) used a three-dimensional, magnetohydrodynamic model of the solar wind with input conditions representative of three different solar epochs: 0.7, 2, and 4.65 Gyr (present day). For the 2-Gyr heliospheric simulations, mean plasma parameters at 1 AU determined by the heliospheric magnetohydrodynamic model include a density of  $30 \text{ cm}^{-3}$ , solar wind speed of 550 km/s, particle temperatures of 17 eV, and interplanetary magnetic field strength of 30 nT (Airapetian & Usmanov, 2016; V. Airapetian, personal communication, November 2017). This corresponds to a solar wind ram pressure of 15 nPa, approximately seven times the present-day value at 1 AU (Dmitriev et al., 2011), which we adopted as input to the hybrid plasma model. For simplicity, we assumed that the solar wind is comprised of only protons ( $\text{H}^+$ ), the upstream interplanetary magnetic field is oriented in the  $+Y$  selenocentric solar ecliptic (SSE; i.e., moon centered,  $+X$  toward the Sun along the Moon-Sun line,  $+Z$  as ecliptic normal, and  $Y$  completing the right-hand set) direction (i.e.,  $\mathbf{B} = [0.0, 30.0, 0.0]$  nT), the solar wind is solely in the  $-X$  SSE direction, and both quantities are steady over the simulation time period.

Tikoo et al. (2017) reported evidence for a  $5 \pm 2 \mu\text{T}$  paleo-magnetic surface field generated by a long-lived lunar dynamo out to  $\sim 1\text{--}2.5$  Gyr. In contrast, paleofields  $\sim 10$  times stronger have been inferred from modern paleomagnetism studies at earlier times ( $>3.5$  Ga; Shea et al., 2012; Suavet et al., 2013). Here, we explore equatorial surface field values of 0.5, 2, and  $5 \mu\text{T}$  and ultimately will show that paleomagnetic fields of these strengths have considerable effects on the solar wind  $\text{H}^+$  surface flux. As for the orientation of the ancient dynamo, numerous recent studies have shown that the dynamo axis may not have been steady in time (Arkani-Hamed & Boutin, 2017; Baek et al., 2019; Nayak et al., 2017; Oliveira & Wiczeorek, 2017; Takahashi & Tsunakawa, 2009). Hence, we model the field as a centered dipole oriented in the  $+Z$  SSE direction (parallel to the lunar spin axis) and also as a dipole perpendicular to the spin axis, in the  $+X/+Y$  SSE plane. For simplicity, we neglect any higher-order (i.e., quadrupole and octupole) contributions to the field, justified by the relatively small size of the lunar core ( $<0.25$  times the lunar radius; Weber et al., 2011), which substantially reduces any higher-order contributions to the surface field. In our analysis, we assume that the angle between the lunar spin axis and ecliptic normal is zero. The present maximal value is  $1.54^\circ$ , and it has remained below  $\sim 10^\circ$  since the Cassini state transition several billion years ago (Siegler et al., 2011).

A theoretical analysis of the pressure balance between the paleo-solar wind and the lunar paleo-magnetic field predicts the formation of a lunar paleo-magnetosphere with a standoff distance,  $d$ , in planetary radii given by

$$d = \left( \frac{2B_o^2}{\mu_o K \rho v_{sw}^2} \right)^{1/6}, \quad (1)$$

where  $B_o$  is the surface magnetic field strength,  $K$  is a value of order unity,  $\rho$  is the solar wind mass density, and  $v_{sw}$  is the solar wind velocity (Kallenrode, 2003). For the parameters modeled here,  $d$  is approximately 1.7, 2.7, and 3.7 lunar radii ( $R_L = 1,738$  km) for equatorial surface field strengths of 0.5, 2.0, and  $5.0 \mu\text{T}$ , respectively, suggesting that the lunar dynamo should have been strong enough to stand off the solar wind and create a magnetosphere. For comparison, these standoff distances are greater than that of Mercury as a function of planetary body radius, whose typical magnetopause location is at approximately  $1.45 R_M$  (where  $R_M = 2,439$  km) (Winslow et al., 2013).

### 3. Paleo-Magnetosphere Results

#### 3.1. Global Morphology

Figure 1 shows the hybrid model results for the interaction of the lunar paleo-magnetic field with the early solar wind for the spin-aligned  $2\text{-}\mu\text{T}$  equatorial surface magnetic field strength case. Panels include (a and b)

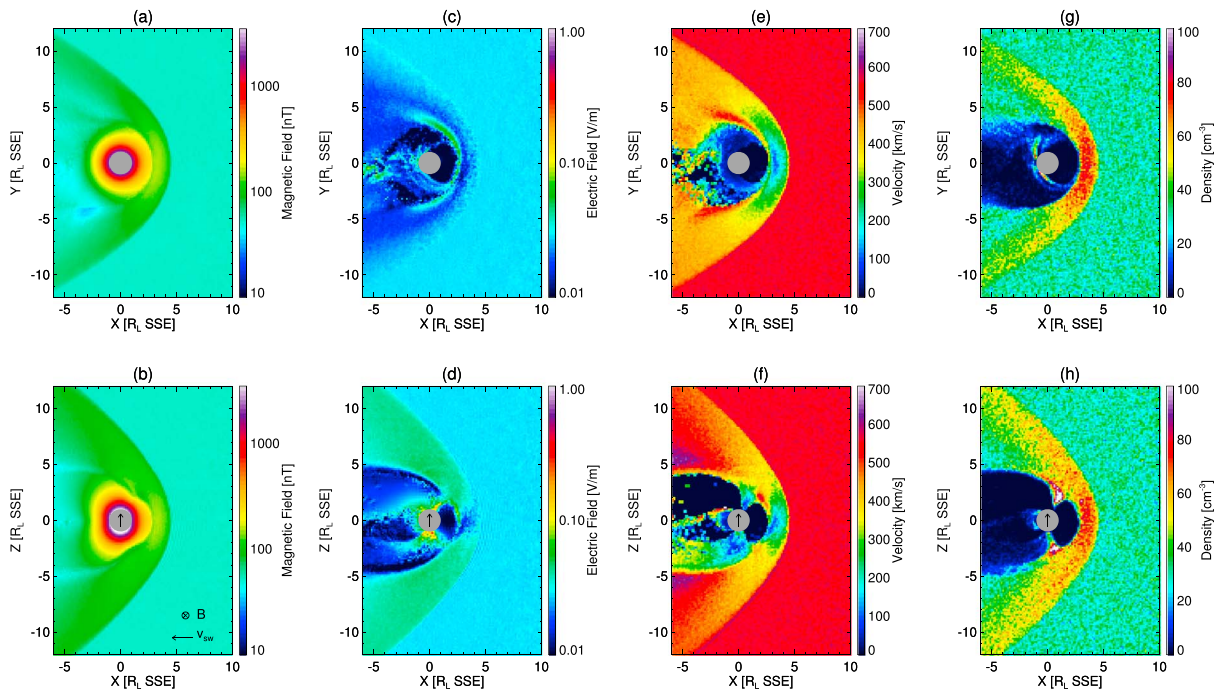


**Figure 1.** The lunar paleo-magnetosphere for the case of a  $2\text{-}\mu\text{T}$  surface field strength in the  $XY$  selenocentric solar ecliptic (SSE) plane (top row) and  $XZ$  SSE plane (bottom row): (a and b) the magnetic field magnitude, (c and d) the electric field magnitude, (e and f) the plasma velocity, and (g and h) the plasma density. In the top panels, the dipole moment is pointed out of the page, and in the bottom panels, the dipole moment is vertical in the plane of the page (arrow in center of figure). The solar wind flows from right to left.

the magnetic field magnitude, (c and d) the electric field magnitude, (e and f) the velocity magnitude, and (g and h) the plasma density, in the  $XY$  SSE and  $XZ$  SSE planes. The simulation results possess all the hallmarks of a standard, magnetospheric interaction with the solar wind. Upstream of the Moon, a bow shock forms near a maximum upstream distance of  $4 R_L$  and a magnetopause forms near  $3 R_L$ , approximately similar to the theoretical calculation of  $2.7 R_L$  from equation (1). The shocked and decelerated solar wind in the lunar magnetosheath is diverted around the lunar magnetosphere, leaving a density void within  $\approx 3 R_L$  upstream of the Moon, corresponding to the region interior to the dayside magnetopause. Solar wind plasma can be seen to access the lunar surface through the magnetospheric cusp regions near the poles, Figure 1h, and trapped particles can be seen in the density and velocity panels on the nightside of the Moon at densities less than  $\approx 30 \text{ cm}^{-3}$  as particles undergo bounce and drift motion and for a partial ring current in the quasi-dipolar region of the lunar magnetosphere.

Figure 2 shows the magnetic field magnitude and plasma density in the  $XZ$  SSE plane for the (a and b)  $0.5\text{-}\mu\text{T}$ , (c and d)  $2\text{-}\mu\text{T}$  (dipole parallel to spin axis), (e and f)  $2\text{-}\mu\text{T}$  (dipole perpendicular to spin axis), and (g and h)  $5\text{-}\mu\text{T}$  surface field strength cases. As expected, an increase in the paleomagnetic surface field strength results in a larger lunar paleo-magnetosphere, with increasing standoff distances in line with the theoretical expectations. The  $0.5\text{-}\mu\text{T}$  case shares many similarities with that of Mercury, which possesses a slightly weaker (and offset) dipole moment yielding equatorial surface fields strengths near  $\approx 300 \text{ nT}$  (Anderson et al., 2011, 2012; Johnson et al., 2012; Winslow et al., 2014). Coincidentally, Mercury is also exposed today to solar wind conditions that are very similar to those calculated by Airapetian and Usmanov (2016) and used here for 2 Ga at 1 AU. The size of the  $0.5\text{-}\mu\text{T}$  magnetosphere has a maximum  $\pm 3 R_L$  vertical extent in the  $YZ$  SSE plane, whereas the  $2\text{-}$  and  $5\text{-}\mu\text{T}$  cases have vertical extents of  $\pm 5$  and  $\pm 6 R_L$ , respectively. Correspondingly, the size of the magnetospheric void (densities less than  $\sim 10 \text{ cm}^{-3}$ ) increases significantly as a function of surface paleofield strength. All four cases also possess slight north-south asymmetries that are noticeable in the relative densities within the magnetospheric cusp regions and in a slight southward displacement of both the dayside magnetosphere and magnetotail. These asymmetries are fundamentally driven by the direction of the interplanetary electric field ( $\mathbf{E} = -\mathbf{v} \times \mathbf{B}$ ), which

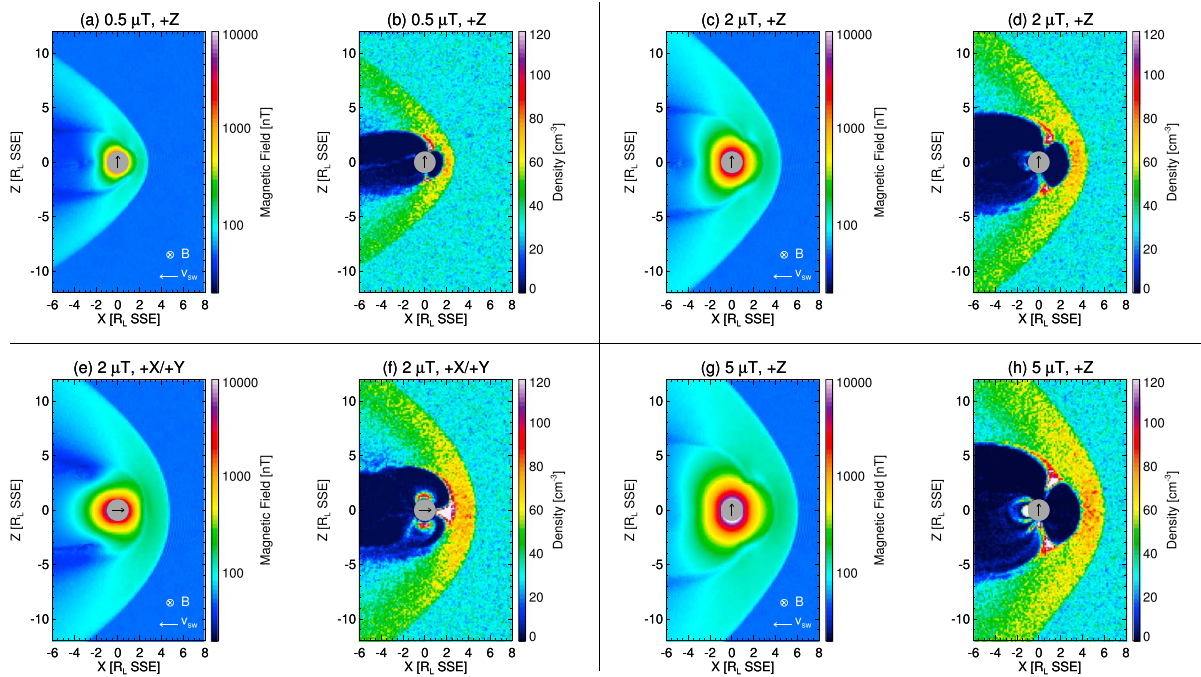


**Figure 2.** A comparison of the magnetic field magnitude and plasma density in the XZ selenocentric solar ecliptic (SSE) plane for three different values of the paleomagnetic surface field strength: (a and b)  $0.5 \mu\text{T}$ , (c and d)  $2 \mu\text{T}$ , (e and f)  $2 \mu\text{T}$  with a spin-perpendicular dipole, and (g and h)  $5 \mu\text{T}$ . Arrows in the center of the figures indicate the orientation of the dipole moment.

generally points upward (+Z) in all simulations. Such electric field-driven asymmetries are also known to occur in the magnetospheres of Venus (e.g., Jarvinen et al., 2013; Zhang et al., 2010) and Mars (e.g., Dubinin et al., 2008) despite the induced, as opposed to intrinsic, nature of these magnetospheres. The density of trapped particles within the closed field-line region of each magnetosphere also increases with the magnetic field strength from  $\sim 1 \text{ cm}^{-3}$  in the  $0.5\text{-}\mu\text{T}$  case to  $>120 \text{ cm}^{-3}$  in the  $5\text{-}\mu\text{T}$  case. We also note the presence of a trapped particle population in the  $2\text{-}\mu\text{T}$  spin-perpendicular case, Figures 2e and 2f, above and below both poles (i.e., centered in the plane of the magnetic equator) and the presence of multiple shells of trapped (or potentially quasi-trapped) particles in the  $5 \mu\text{T}$  case, Figure 2h. While beyond the scope of the current paper, an analysis of the population and stability of these trapped particle belts along with a comparison to analogous work at Earth (e.g., Klida & Fritz, 2009) and Mercury (e.g., Walsh et al., 2013; Yagi et al., 2017) is identified as a promising line of inquiry.

### 3.2. Solar Wind Ion Implantation

The hybrid model also tracks the flux of solar wind ions that access the lunar surface as a function of impact location on the lunar surface. For each of the runs shown in Figure 2, we compiled the average solar wind flux to the surface and averaged over longitudes (since the lunar spin should expose selenographic longitudes to all sectors of the paleo-magnetosphere over long time periods). Figure 3 shows the average flux to the lunar surface as a function of latitude for (a) the  $0.5\text{-}$ ,  $2\text{-}$ , and  $5\text{-}\mu\text{T}$  spin-aligned cases and (b) the  $2\text{-}\mu\text{T}$  spin-aligned and spin-perpendicular cases. In Figure 3a, the model predicts that more flux precipitates to the lunar polar regions and less to the equatorial region for all three paleofield strengths compared to the unmagnetized case ( $0 \mu\text{T}$ , black curve). Such a pattern is comparable to that predicted and observed at Mercury (Delitsky et al., 2017; Massetti et al., 2003; Raines et al., 2014). Furthermore, greater surface precipitation is observed in the polar regions for higher paleomagnetic field strength (i.e., the  $5\text{-}\mu\text{T}$  case shows the most flux to the polar regions) as the paleo-magnetosphere cusp regions funnel relatively more flux to the poles. At the equator, the  $\text{H}^+$  flux is reduced by at least an order of magnitude (i.e., in the  $2\text{-}\mu\text{T}$  case) and completely arrested within  $20^\circ$  of the equator by a field of  $5 \mu\text{T}$ . We also note dips in the surface flux in all three cases ( $0.5$ ,  $2$ , and  $5 \mu\text{T}$ ) at approximate latitudes of  $50^\circ$ ,  $60^\circ$ , and  $70^\circ$  N/S, respectively, corresponding to the outer regions of the closed magnetospheric field lines that cannot efficiently trap particles (and

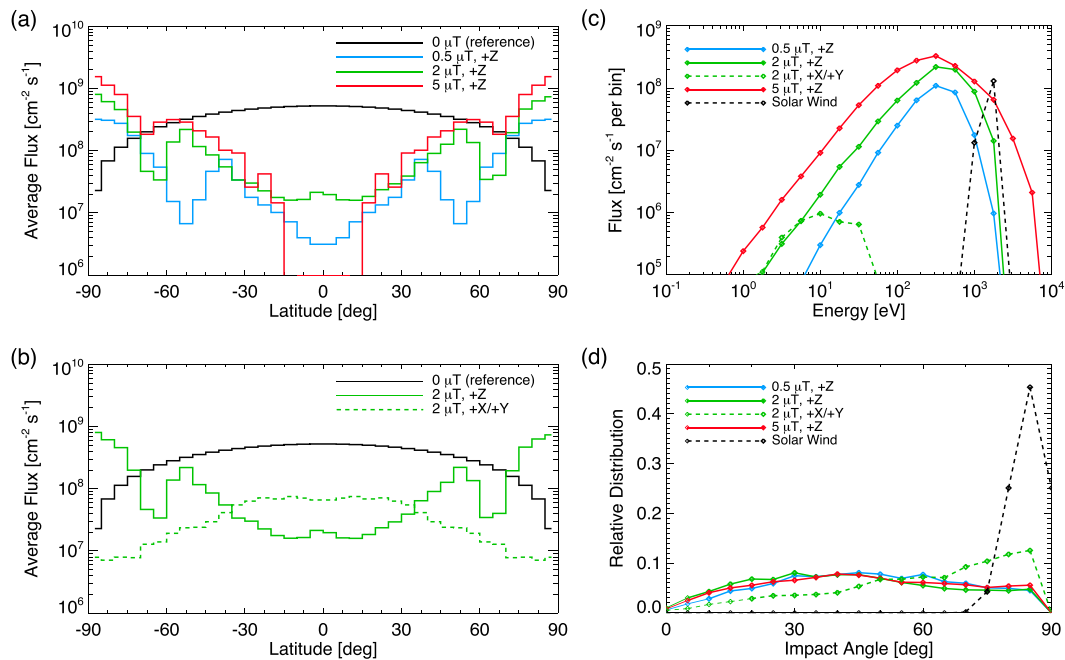


**Figure 3.** (a) Flux of  $H^+$  to the surface for three paleomagnetic surface field strengths and the reference field-free case. (b) Flux of  $H^+$  to the surface for a paleomagnetic surface field of 2  $\mu T$ , with the dipole axis parallel (+Z) and perpendicular (+X/+Y) to the spin axis (see Figures 2c–2f). The (c) energy and (d) impact angle distributions with respect to the local surface normal of  $H^+$  in regions of latitude greater than 80° N/S for all cases.

subsequently have them precipitate to the surface), presumably due to effects such as magnetopause shadowing. In Figure 3b, the spin-aligned (solid green curve) and spin-perpendicular (dashed green curve) 2- $\mu T$  cases show strong differences, with the spin-perpendicular case showing 2 orders of magnitude less flux to the polar region and approximately a factor of 3 more flux to the equatorial region than the spin-parallel case. Notably, the spin-perpendicular case has fluxes nearly an order of magnitude less than the unmagnetized case (black curve) over all longitudes.

Overall, we find that the total surface integrated flux of  $H^+$  to the Moon decreases to 9%, 18%, and 33% of the incident solar wind flux compared to the nonmagnetized case, for spin-aligned dipole fields of 0.5, 2, and 5  $\mu T$ , respectively (for the 2  $\mu T$  spin-perpendicular case, the total surface flux decreases to 11% of the nonmagnetized case). While somewhat counterintuitive, the *increase* in total precipitating flux with increasing paleomagnetic field strength is due to greater channeling of solar wind fluxes into the magnetospheric cusp regions as noted above; however, we also expect that total solar wind precipitation will again decline for field strengths much greater than 5  $\mu T$  as the loss cones within the cusp regions continue to narrow. While not shown, we ran additional 0.1- and 0.25- $\mu T$  field strengths and found greater precipitation than the 0.5- $\mu T$  case. Hence, shielding effectiveness peaks at 0.5  $\mu T$ , for field strengths between 0.5 and 5  $\mu T$ . Overall, this peak is due to two competing effects: (i) stronger surface field strengths better shield solar wind plasma from directly striking the lunar surface versus (ii) stronger surface field strengths funnel more solar wind plasma into the cusp regions, thereby offsetting the shielding from the former effect (as stated above). Nevertheless, if the dynamo were dominantly dipolar as simulated here and within the surface field strength measured by Tikoo et al. (2017) of  $5 \pm 2 \mu T$ , the Moon's surface would have been mostly shielded from solar wind  $H^+$  for the life of the dynamo.

In addition to the overall flux, we have calculated the impact energy and angular distributions of solar wind protons in the polar regions (defined as latitudes poleward of 80°N/S). Figure 3c shows the energy distribution of the precipitating flux of solar wind protons in the polar regions for all four paleomagnetic cases shown in Figure 2 along with the energy distribution expected in the case of no paleomagnetic field (i.e., the undisturbed solar wind). For the three spin-aligned cases (solid curves), the energy distribution is slower and hotter than the solar wind, due to the upstream bow shock that slows and heats the solar wind before it enters the magnetospheric cusp regions and precipitates to the surface. In

agreement with Figure 3a, the overall magnitude of the flux in the polar regions for the paleo-magnetospheric cases is greater than that of the unmagnetized case. In contrast, the energy distribution for the 2- $\mu$ T spin-perpendicular case is not only significantly reduced in flux (as expected from Figure 3b) but also significantly lower in energy (1-50 eV). The angular distribution of precipitating solar wind ions, Figure 3d, shows significant differences between the undisturbed solar wind, which mainly impacts at angles between 75-90° with respect to the local surface normal, and the four paleo-magnetospheric cases, which impact at all angles nearly isotropically. Thus, in the presence of a dynamo field the solar wind flux has essentially direct access to the lunar polar regions. Such conditions may have prevented the formation of the unique electric field environment that is believed to be established in present-day polar craters when the nominal undisturbed solar wind passes over them at shallow angles (Zimmerman et al., 2012) and also may increase the rate at which polar volatile erosion occurs (e.g., Crider & Vondrak, 2003a; Crider & Vondrak, 2003b; Hurley et al., 2012; Zimmerman et al., 2013)

#### 4. Discussion and Conclusions

Our simulation results suggest a fundamentally different paradigm for the lunar-solar wind interaction throughout much of Moon's lifetime, with the closest analog being that of present-day Mercury. One may in fact expect that the Moon experienced a wealth of plasma phenomena similar to that observed at Mercury, such as heavily solar wind-driven magnetospheric dynamics (Dibraccio et al., 2013; Exner et al., 2018; Jia et al., 2019; Slavin et al., 2010, 2012, 2014; Sun et al., 2015), the circulation of ionized planetary material (Raines et al., 2013; Zurbuchen et al., 2008; Zurbuchen et al., 2011), and the interaction between magnetospheric and inductive fields from the lunar interior (Johnson et al., 2016; Korth et al., 2017). In our analysis here, we neglected the interaction of the ancient terrestrial magnetosphere with the putative lunar paleo-magnetosphere during lunar transits across the magnetotail; however, it is possible that the different distributions of plasma in the terrestrial magnetosheath and magnetotail at downtail distances (Poppe, Farrell et al., 2018) could alter the magnetospheric interaction of the lunar paleo-magnetosphere during terrestrial magnetotail transits, especially since magnetotail plasmas are subsonic and of much lower density. In particular, the subsonic nature of the ambient plasma may yield an interaction more typical of Ganymede, which is embedded in the subsonic (and usually sub-Aflvénic) jovian flow (e.g., Fatemi et al., 2016; Jia et al., 2008; Kivelson et al., 2004; Paty & Winglee, 2004). Additionally, the lunar paleo-magnetosphere may also have affected the implantation rate of terrestrial ionospheric material at the Moon (Mortimer et al., 2016; Ozima et al., 2005; Poppe et al., 2016; Terada et al., 2017).

The reduced global flux of  $H^+$  and increased polar flux suggested by these results may modify the understanding of hydrogen accumulation at the lunar poles in several ways. First, if the present-day polar hydrogen is an accumulation of OH/ $H_2O$  produced by solar wind  $H^+$  implantation and subsequent migration from elsewhere on the Moon (e.g., the equatorial region; Butler, 1997; Crider & Vondrak, 2000; Crider & Vondrak, 2002), then our results suggest that OH/ $H_2O$  accumulation at the poles would be reduced over the lifetime of the lunar dynamo. This would imply the polar hydrogen deposits developed in the last 1-2 billion years after the dynamo fully ceased. Second, other hypotheses suggest the polar hydrogen is directly implanted  $H^+$  (Starukhina, 2000; and reviewed by Feldman et al., 2001). If this process is feasible, our results suggest that the Moon's magnetosphere may have actually enhanced its efficiency in the case of a spin-aligned dipole. However, the increased flux of polar  $H^+$  in the presence of a lunar paleo-magnetosphere could also have increased weathering and destruction of any existing volatile deposits (Crider & Vondrak, 2003b; Delitsky et al., 2017; Hurley et al., 2012). Thirdly, if the present-day polar hydrogen is due to  $H_2O$  vapor released from micrometeoroid water (e.g., Füri et al., 2012), it is likely that the presence of a paleo-magnetosphere had a negligible effect on accumulation rates, aside from possible magnetospheric interactions with photo-ionized exospheric molecules. Finally, the recent suggestion of a dense (tens to hundreds of Pa), transient atmosphere on the early Moon (~4.0 – 1.0 Ga) produced by volcanic outgassing (Needham & Kring, 2017) may further complicate the early lunar-solar wind interaction. If such a dense atmosphere truly existed during this period, the Moon may have more resembled a hybrid of present-day Mars (with its ~600-Pa  $CO_2$  dominated atmosphere) and Mercury (with its ~300-nT surface magnetic field), a situation for which our solar system has no current analog. The ionization, circulation, and potential implantation of volatile species at the lunar poles under such conditions have not been previously considered and represents a topic of future work. Nevertheless, our initial investigation into the paleo-magnetospheric interaction of the Moon with the

early solar wind has suggested that such an interaction must be considered when assessing the evolution of volatile material at the Moon over the course of its history.

#### Acknowledgments

This work was supported by the BK21 plus program through the National Research Foundation (NRF), funded by the Ministry of Education of Korea. IGB and ARP acknowledge support from NASA grant 80NSSC19K0560 A. R. P. acknowledges NASA's Solar System Exploration Research Virtual Institute, Grant NNX14AG16A. Modeling results are available in the UC Berkeley Data Repository website (<http://dash.berkeley.edu>).

#### References

- Airapetian, V. S., A. Gloer, and W. Danchi (2014), Magnetic interaction of a super-CME with the Earth's magnetosphere: Scenario for young Earth, *Proceedings of the 18th Cambridge Workshop on Cool Stars, Stellar Systems, and the Sun*, PDF available at <https://arxiv.org/abs/1410.7355>.
- Airapetian, V. S., & Usmanov, A. V. (2016). Reconstructing the solar wind from its early history to current epoch. *The Astrophysical Journal*, 817(2), L24. <https://doi.org/10.3847/2041-8205/817/2/L24>
- Anderson, B. J., Johnson, C. L., Korth, H., Purucker, M. E., Winslow, R. M., Slavlin, J. A., et al. (2011). The global magnetic field of Mercury from MESSENGER Orbital Observations. *Science*, 333(6051), 1859–1862. <https://doi.org/10.1126/science.1211001>
- Anderson, B. J., Johnson, C. L., Korth, H., Winslow, R. M., Borovsky, J. E., Purucker, M. E., et al. (2012). Low-degree structure in Mercury's planetary magnetic field. *Journal of Geophysical Research*, 117, E00L12. <https://doi.org/10.1029/2012JE004159>
- Arkani-Hamed, J., & Boutin, D. (2017). South Pole Aitken Basin magnetic anomalies: Evidence for the true polar wander of Moon and a lunar dynamo reversal. *Journal of Geophysical Research: Planets*, 122, 1195–1216. <https://doi.org/10.1002/2016JE005234>
- Baek, S.-M., Kim, K.-H., Garrick-Bethell, I., & Jin, H. (2019). Magnetic anomalies within the Crisium basin: Magnetization directions, source depths, and ages. *Journal of Geophysical Research: Planets*, 124, 223–242. <https://doi.org/10.1029/2018je005678>
- Bogard, D. D., Nyquist, L. E., Hirsch, W. C., & Moore, D. R. (1973). Trapped solar and cosmogenic noble gas abundances in Apollo 15 and 16 deep drill samples. *Earth and Planetary Science Letters*, 21(1), 52–69. [https://doi.org/10.1016/0012-821X\(73\)90225-2](https://doi.org/10.1016/0012-821X(73)90225-2)
- Butler, B. J. (1997). The migration of volatiles on the surfaces of Mercury and the Moon. *Journal of Geophysical Research*, 102(E8), 19,283–19,291. <https://doi.org/10.1029/97JE01347>
- Colaprete, A., Schultz, P., Heldmann, J., Wooden, D., Shirley, M., Ennico, K., et al. (2010). Detection of water in the LCROSS Ejecta Plume. *Science*, 330(6003), 463–468. <https://doi.org/10.1126/science.1186986>
- Cooper, J. F., Johnson, R. E., Mauk, B. H., Garrett, H. B., & Gehrels, N. (2001). Energetic ion and electron irradiation of the icy Galilean satellites. *Icarus*, 149(1), 133–159. <https://doi.org/10.1006/icar.2000.6498>
- Cournède, C., Gattacceca, J., & Rochette, P. (2012). Magnetic study of large Apollo samples: Possible evidence for an ancient centered dipolar field on the Moon. *Earth and Planetary Science Letters*, 331, 31–42. <https://doi.org/10.1016/j.epsl.2012.03.004>
- Crider, D. H., & Vondrak, R. R. (2000). The solar wind as a possible source of lunar polar hydrogen deposits. *Journal of Geophysical Research*, 105(E11), 26,773–26,782. <https://doi.org/10.1029/2000JE001277>
- Crider, D. H., & Vondrak, R. R. (2002). Hydrogen migration to the lunar poles by solar wind bombardment of the moon. *Advances in Space Research*, 30(8), 1869–1874. [https://doi.org/10.1016/S0273-1177\(02\)00493-3](https://doi.org/10.1016/S0273-1177(02)00493-3)
- Crider, D. H., & Vondrak, R. R. (2003a). Space weathering effects on lunar cold trap deposits. *Journal of Geophysical Research*, 108(E7), 5079. <https://doi.org/10.1029/2002JE002030>
- Crider, D. H., & Vondrak, R. R. (2003b). Space weathering of ice layers in lunar cold traps. *Advances in Space Research*, 31(11), 2293–2298. [https://doi.org/10.1016/S0273-1177\(03\)00530-1](https://doi.org/10.1016/S0273-1177(03)00530-1)
- Delitsky, M. L., Paige, D. A., Siegler, M. A., Harju, E. R., Schriver, D., Johnson, R. E., & Travnicek, P. (2017). Ices on Mercury: Chemistry of volatiles in permanently cold areas of Mercury's north polar region. *Icarus*, 281, 19–31. <https://doi.org/10.1016/j.icarus.2016.08.006>
- Dibraccio, G. A., Slavlin, J. A., Boardsen, S. A., Anderson, B. J., Korth, H., Zurbuchen, T. H., et al. (2013). MESSENGER observations of magnetopause structure and dynamics at Mercury. *Journal of Geophysical Research: Space Physics*, 118, 997–1008. <https://doi.org/10.1002/jgra.50123>
- Dmitriev, A. V., Suvorova, A. V., & Veselovsky, I. S. (2011). Statistical characteristics of the heliospheric plasma and magnetic field at Earth's orbit. In H. E. Johannson (Ed.), *Handbook on Solar Wind: Effects, Dynamics, and Interactions*, (pp. 81–144). New York, NY, USA: NOVA Science Publishers.
- Domingue, D. L., Chapman, C. R., Killen, R. M., Zurbuchen, T. H., Gilbert, J. A., Sarantos, M., et al. (2014). Mercury's weather-beaten surface: Understanding Mercury in the context of lunar and asteroidal space weathering studies. *Space Science Reviews*, 181(1–4), 121–214. <https://doi.org/10.1007/s11214-014-0039-5>
- Dubinin, E., Chantaur, G., Fraenz, M., Modolo, R., Woch, J., Roussos, E., et al. (2008). Asymmetry of plasma fluxes at Mars. ASPERA-3 observations and hybrid simulations. *Planetary Space Science*, 56(6), 832–835. <https://doi.org/10.1016/j.pss.2007.12.006>
- Dyal, P., & Parkin, C. W. (1971). Electrical conductivity and temperature of the lunar interior from magnetic transient-response measurements. *Journal of Geophysical Research*, 76(25), 5947–5969. <https://doi.org/10.1029/JA076i025p05947>
- Eberhardt, P., et al. (1972). Trapped solar wind noble gases in Apollo 12 lunar fines 12001 and Apollo 11 breccia 10046, in *Lunar and Planetary Science Conference Proceedings*, edited by A. E. Metzger, pp. 1821–1856.
- Eugster, O., Terribilini, D., Polnau, E., & Kramers, J. (2001). The antiquity indicator argon-40/argon-36 for lunar surface samples calibrated by uranium-235-xenon-136 dating. *Meteoritics and Planetary Science*, 36(8), 1097–1115. <https://doi.org/10.1111/j.1945-5100.2001.tb01947.x>
- Evans, A. J., Tikoo, S. M., & Andrews-Hanna, J. C. (2018). The case against an early lunar dynamo powered by core convection. *Geophysical Research Letters*, 45(1), 98–107. <https://doi.org/10.1002/2017GL075441>
- Exner, W., Heyner, D., Liuzzo, L., Motschmann, U., Shiota, D., Kusano, K., & Shibayama, T. (2018). Coronal mass ejection hits Mercury: A I.K.E.F. hybrid-code results compared to MESSENGER data. *Planetary Space Science*, 153, 89–99. <https://doi.org/10.1016/j.pss.2017.12.016>
- Fatemi, S., Fuqua, H. A., Poppe, A. R., Delory, G. T., Halekas, J. S., Farrell, W. M., & Holmström, M. (2015). On the confinement of lunar induced magnetic fields. *Geophysical Research Letters*, 42, 6931–6938. <https://doi.org/10.1002/2015GL065576>
- Fatemi, S., Poirier, N., Holmström, M., Lindkvist, J., Wieser, M., & Barabash, S. (2018). A modelling approach to infer the solar wind dynamic pressure from magnetic field observations inside Mercury's magnetosphere. *Astronomy and Astrophysics*, 614, A132. <https://doi.org/10.1051/0004-6361/201832764>
- Fatemi, S., & Poppe, A. R. (2018). Solar wind plasma interaction with asteroid 16 Psyche: Implication for Formation Theories. *Geophysical Research Letters*, 45(1), 39–48. <https://doi.org/10.1002/2017GL073980>
- Fatemi, S., Poppe, A. R., Delory, G. T., & Farrell, W. M. (2017). AMITIS: A 3D GPU-based hybrid-PIC model for space and plasma physics. *Journal of Physics: Conference Series*, 837.



- Fatemi, S., Poppe, A. R., Khurana, K. K., Holmström, M., & Delory, G. T. (2016). On the formation of Ganymede's surface brightness asymmetries: Kinetic simulations of Ganymede's magnetosphere. *Geophysical Research Letters*, *43*, 4745–4754. <https://doi.org/10.1002/2016GL068363>
- Feldman, W. C., Maurice, S., Lawrence, D. J., Little, R. C., Lawson, S. L., Gasnault, O., et al. (2001). Evidence for water ice near the lunar poles. *Journal of Geophysical Research*, *106*(E10), 23,231–23,251. <https://doi.org/10.1029/2000JE001444>
- Fuller, M., & Cisowski, S. M. (1987). Lunar paleomagnetism. *Geomagnetism*, *307*(2), 307–455.
- Füri, E., Marty, B., & Assonov, S. S. (2012). Constraints on the flux of meteoritic and cometary water on the Moon from volatile element (N-Ar) analyses of single lunar soil grains, Luna 24 core. *Icarus*, *218*(1), 220–229. <https://doi.org/10.1016/j.icarus.2011.11.037>
- Garrick-Bethell, I., Perera, V., Nimmo, F., & Zuber, M. T. (2014). The tidal-rotational shape of the Moon and evidence for polar wander. *Nature*, *512*(7513), 181–184. <https://doi.org/10.1038/nature13639>
- Garrick-Bethell, I., Poppe, A. R., & Fatemi, S. (2018). The lunar paleomagnetosphere: Insights into field enhancements, isotopic fractionation of the ancient solar wind, and volatile production, in Lunar and Planetary Science Conference, 49th, edited, p. 2439.
- Garrick-Bethell, I., Weiss, B. P., Tikoo, S. M., Shuster, D. L., & Tremblay, M. M. (2017). Further evidence of early lunar magnetism from troctolite 76535. *Journal of Geophysical Research: Planets*, *122*, 76–93. <https://doi.org/10.1002/2016je005154>
- Gershman, D. J., Raines, J. M., Slavin, J. A., Zurbuchen, T. H., Sundberg, T., Boardsen, S. A., et al. (2015). MESSENGER observations of multiscale Kelvin-Helmholtz vortices at Mercury. *Journal of Geophysical Research: Space Physics*, *120*, 4354–4368. <https://doi.org/10.1002/2014JA020903>
- Hurley, D. M., Lawrence, D. J., Bussey, D. B. J., Vondrak, R. R., Elphic, R. C., & Gladstone, G. R. (2012). Two-dimensional distribution of volatiles in the lunar regolith from space weathering simulations. *Geophysical Research Letters*, *39*, L09203. <https://doi.org/10.1029/2012GL051105>
- Jarvinen, R., Kallio, E., & Dyadechkin, S. (2013). Hemispheric asymmetries of the Venus plasma environment. *Journal Geophysical Research: Space Physics*, *118*, 4551–4563. <https://doi.org/10.1002/jgra.50387>
- Jia, X., Slavin, J. A., Poh, G., DiBraccio, G. A., Toth, G., Chen, Y., et al. (2019). MESSENGER observations and global simulations of highly compressed magnetosphere events at Mercury. *Journal Geophysical Research: Space Physics*, *124*, 229–247. <https://doi.org/10.1029/2018JA026166>
- Jia, X., Walker, J., Kivelson, M. G., Khurana, K. K., & Linker, J. A. (2008). Three-dimensional MHD simulations of Ganymede's magnetosphere. *Journal Geophysical Research*, *113*, A06212. <https://doi.org/10.1029/2007JA012748>
- Johnson, C. L., Philpott, L. C., Anderson, B. J., Korth, H., Hauck, S. A., Heyner, D., et al. (2016). MESSENGER observations of induced magnetic fields in Mercury's core. *Geophysical Research Letters*, *43*, 2436–2444. <https://doi.org/10.1002/2015GL067370>
- Johnson, C. L., Purucker, M. E., Korth, H., Anderson, B. J., Winslow, R. M., al Asad, M. M. H., et al. (2012). MESSENGER observations of Mercury's magnetic field structure. *Journal of Geophysical Research*, *117*, E00L14. <https://doi.org/10.1029/2012JE004217>
- Joy, K. H., Kring, D. A., Bogard, D. D., McKay, D. S., & Zolensky, M. E. (2011). Re-examination of the formation ages of the Apollo 16 regolith breccias. *Geochimica et Cosmochimica Acta*, *75*(22), 7208–7225. <https://doi.org/10.1016/j.gca.2011.09.018>
- Kallenrode, M.-B. (2003). *Space physics: An introduction to plasmas and particles in the heliosphere and magnetospheres*, (Vol. 482). Springer.
- Kivelson, M. G., Bagenal, F., Kurth, W. S., Neubauer, F. M., Paranicas, C., & Saur, J. (2004). Magnetospheric interactions with satellites. In F. Bagenal, T. Dowling, & W. McKinnon (Eds.), *Jupiter: The planet, satellites, and magnetosphere*, (pp. 513–536). Cambridge University Press.
- Klida, M. M., & Fritz, T. A. (2009). The Earth's magnetopause as a source and sink for equatorial nightside energetic charged particles. *Annals of Geophysics*, *27*(11), 4305–4316. <https://doi.org/10.5194/angeo-27-4305-2009>
- Korth, H., Johnson, C. L., Philpott, L., Tsyganenko, N. A., & Anderson, B. J. (2017). A dynamic model of Mercury's magnetospheric magnetic field. *Geophysical Research Letters*, *44*, 10,147–10,154. <https://doi.org/10.1002/2017GL074699>
- Massetti, S., Orsini, S., Milillo, A., Mura, A., De Angelis, E., Lammer, H., & Wurz, P. (2003). Mapping of the cusp plasma precipitation on the surface of Mercury. *Icarus*, *166*(2), 229–237. <https://doi.org/10.1016/j.icarus.2003.08.005>
- Mortimer, J., Verchovsky, A. B., & Anand, M. (2016). Predominantly non-solar origin of nitrogen in lunar soils. *Geochimica et Cosmochimica Acta*, *193*, 36–53. <https://doi.org/10.1016/j.gca.2016.08.006>
- Nayak, M., Hemingway, D., & Garrick-Bethell, I. (2017). Magnetic anomalies of the South Pole-Aitken Basin: Implications for true polar wander and the history of the lunar dynamo. *Icarus*, *286*, 153–192. <https://doi.org/10.1016/j.icarus.2016.09.038>
- Needham, D. H., & Kring, D. A. (2017). Lunar volcanism produced a transient atmosphere around the ancient Moon. *Earth and Planetary Science Letters*, *478*, 175–178. <https://doi.org/10.1016/j.epsl.2017.09.002>
- Oliveira, J. S., & Wiczeorek, M. A. (2017). Testing the axial dipole hypothesis for the Moon by modeling the direction of crustal magnetization. *Journal of Geophysical Research: Planets*, *122*, 383–399. <https://doi.org/10.1002/2016JE005199>
- Ozima, M., Seki, K., Terada, N., Miura, Y. N., Podosek, F. A., & Shinagawa, H. (2005). Terrestrial nitrogen and noble gases in lunar soils. *Nature*, *436*(7051), 655–659. <https://doi.org/10.1038/nature03929>
- Paty, C., & Winglee, R. (2004). Multi-fluid simulations of Ganymede's magnetosphere. *Geophysical Research Letters*, *31*, L24806. <https://doi.org/10.1029/2004GL021220>
- Pieters, C. M., Goswami, J. N., Clark, R. N., Annadurai, M., Boardman, J., Buratti, B., et al. (2009). Character and spatial distribution of OH/H<sub>2</sub>O on the surface of the Moon Seen by M3 on Chandrayaan-1. *Science*, *326*(5952), 568–572. <https://doi.org/10.1126/science.1178658>
- Poppe, A. R., Farrell, W. M., & Halekas, J. S. (2018). Formation timescales of amorphous rims on lunar grains derived from ARTEMIS observations. *Journal of Geophysical Research: Planets*, *123*, 37–46. <https://doi.org/10.1002/2017JE005426>
- Poppe, A. R., Fatemi, S., & Khurana, K. K. (2018). Thermal and energetic ion dynamics in Ganymede's magnetosphere. *Journal of Geophysical Research: Space Physics*, *123*, 4614–4637. <https://doi.org/10.1029/2018JA025312>
- Poppe, A. R., Fillingim, M. O., Halekas, J. S., Raeder, J., & Angelopoulos, V. (2016). ARTEMIS observations of terrestrial ionospheric molecular ion outflow at the Moon. *Geophysical Research Letters*, *43*, 6749–6758. <https://doi.org/10.1002/2016GL069715>
- Raines, J. M., DiBraccio, G. A., Cassidy, T. A., Delcourt, D. C., Fujimoto, M., Jia, X., et al. (2015). Plasma sources in planetary magnetospheres: Mercury. *Space Science Reviews*, *192*(1-4), 91–144. <https://doi.org/10.1007/s11214-015-0193-4>
- Raines, J. M., Gershman, D. J., Slavin, J. A., Zurbuchen, T. H., Korth, H., Anderson, B. J., & Solomon, S. C. (2014). Structure and dynamics of Mercury's magnetospheric cusp: MESSENGER measurements of protons and planetary ions. *Journal of Geophysical Research: Space Physics*, *119*, 6587–6602. <https://doi.org/10.1002/2014JA020120>

- Raines, J. M., Gershman, D. J., Zurbuchen, T. H., Sarantos, M., Slavin, J. A., Gilbert, J. A., et al. (2013). Distribution and compositional variations of plasma ions in Mercury's space environment: The first three Mercury years of MESSENGER observations. *Journal of Geophysical Research: Space Physics*, *118*, 1604–1619. <https://doi.org/10.1029/2012JA018073>
- Raines, J. M., Slavin, J. A., Zurbuchen, T. H., Gloeckler, G., Anderson, B. J., Baker, D. N., et al. (2011). MESSENGER observations of the plasma environment near Mercury. *Planetary and Space Science*, *59*(15), 2004–2015. <https://doi.org/10.1016/j.pss.2011.02.004>
- Shea, E. K., Weiss, B. P., Cassata, W. S., Shuster, D. L., Tikoo, S. M., Gattacceca, J., et al. (2012). A long-lived lunar core dynamo. *Science*, *335*(6067), 453–456. <https://doi.org/10.1126/science.1215359>
- Siegler, M. A., Bills, B. G., & Paige, D. A. (2011). Effects of orbital evolution on lunar ice stability. *Journal of Geophysical Research*, *116*, E03010. <https://doi.org/10.1029/2010JE003652>
- Siegler, M. A., Miller, R. S., Keane, J. T., Laneuville, M., Paige, D. A., Matsuyama, I., et al. (2016). Lunar true polar wander inferred from polar hydrogen. *Nature*, *531*(7595), 480–484. <https://doi.org/10.1038/nature17166>
- Slavin, J. A., Anderson, B. J., Baker, D. N., Benna, M., Boardsen, S. A., Gloeckler, G., et al. (2010). MESSENGER observations of extreme loading and unloading of Mercury's magnetic tail. *Science*, *329*(5992), 665–668. <https://doi.org/10.1126/science.1188067>
- Slavin, J. A., DiBraccio, G. A., Gershman, D. J., Imber, S. M., Poh, G. K., Raines, J. M., et al. (2014). MESSENGER observations of Mercury's dayside magnetosphere under extreme solar wind conditions. *Journal of Geophysical Research: Space Physics*, *119*, 8087–8116. <https://doi.org/10.1002/2014JA020319>
- Slavin, J. A., Imber, S. M., Boardsen, S. A., DiBraccio, G. A., Sundberg, T., Sarantos, M., et al. (2012). MESSENGER observations of a flux-transfer-event shower at Mercury. *Journal of Geophysical Research*, *117*, A00M06. <https://doi.org/10.1029/2012JA017926>
- Sonett, C. P., Schubert, G., Smith, B. F., Schwartz, K., & Colburn, D. S. (1971). Lunar electrical conductivity from Apollo 12 magnetometer measurements: Compositional and thermal inferences. *Lunar and Planetary Science Conference Proceedings*, *3*, 2415–2431.
- Starukhina, L. V. (2000). On the origin of excess hydrogen at the lunar poles. *Solar System Research*, *34*, 215.
- Suavet, C., Weiss, B. P., Cassata, W. S., Shuster, D. L., Gattacceca, J., Chan, L., et al. (2013). Persistence and origin of the lunar core dynamo. *Proceedings of the National Academy of Science*, *110*(21), 8453–8458. <https://doi.org/10.1073/pnas.1300341110>
- Sun, W.-J., Slavin, J. A., Fu, S., Raines, J. M., Zong, Q. G., Imber, S. M., et al. (2015). MESSENGER observations of magnetospheric substorm activity in Mercury's near magnetotail. *Geophysical Research Letters*, *42*, 3692–3699. <https://doi.org/10.1002/2015GL064052>
- Sunshine, J. M., Farnham, T. L., Feaga, L. M., Groussin, O., Merlin, F., Milliken, R. E., & A'Hearn, M. F. (2009). Temporal and spatial variability of lunar hydration as observed by the deep impact spacecraft. *Science*, *326*(5952), 565–568. <https://doi.org/10.1126/science.1179788>
- Takahashi, F., & Tsunakawa, H. (2009). Thermal core-mantle coupling in an early lunar dynamo: Implications for a global magnetic field and magnetosphere of the early Moon. *Geophysical Research Letters*, *36*, L24202. <https://doi.org/10.1029/2009GL041221>
- Terada, K., Yokota, S., Saito, Y., Kitamura, N., Asamura, K., & Nishino, M. N. (2017). Biogenic oxygen from Earth transported to the Moon by a wind of magnetospheric ions. *Nature Astronomy*, *1*(2). <https://doi.org/10.1038/s41550-016-0026>
- Tikoo, S. M., Weiss, B. P., Shuster, D. L., Suavet, C., Wang, H., & Grove, T. L. (2017). A two-billion-year history for the lunar dynamo. *Science Advances*, *3*(8), e1700207. <https://doi.org/10.1126/sciadv.1700207>
- Walsh, B. M., Ryou, A. S., Sibeck, D. G., & Alexeev, I. I. (2013). Energetic particle dynamics in Mercury's magnetosphere. *Journal of Geophysical Research: Space Physics*, *118*, 1992–1999. <https://doi.org/10.1002/jgra.50266>
- Weber, R. C., Lin, P.-Y., Garner, E. J., Williams, Q., & Lognonné, P. (2011). Seismic detection of the lunar core. *Science*, *331*(6015), 309–312. <https://doi.org/10.1126/science.1199375>
- Weiss, B. P., & Tikoo, S. M. (2014). The lunar dynamo. *Science*, *346*, 1198.
- Wieler, R. (2016). Do lunar and meteoritic archives record temporal variations in the composition of solar wind noble gases and nitrogen? A reassessment in the light of Genesis data. *Chemie der Erde*, *76*(4), 463–480. <https://doi.org/10.1016/j.chemer.2016.06.001>
- Winslow, R. M., Anderson, B. J., Johnson, C. L., Slavin, J. A., Korth, H., Purucker, M. E., et al. (2013). Mercury's magnetopause and bow shock from MESSENGER Magnetometer observations. *Journal of Geophysical Research: Space Physics*, *118*, 2213–2227. <https://doi.org/10.1002/jgra.50237>
- Winslow, R. M., Johnson, C. L., Anderson, B. J., Gershman, D. J., Raines, J. M., Lillis, R. J., et al. (2014). Mercury's surface magnetic field determined from proton-reflection magnetometry. *Geophysical Research Letters*, *41*, 4463–4470. <https://doi.org/10.1002/2014GL060258>
- Wood, B. E., Müller, H.-R., Zank, G. P., Linsky, J. L., & Redfield, S. (2005). New mass-loss measurements from astrospheric Ly $\alpha$  absorption. *The Astrophysical Journal Letters*, *628*(2), L143–L146. <https://doi.org/10.1086/432716>
- Yagi, M., Seki, K., Matsumoto, Y., Delcourt, D. C., & Leblanc, F. (2017). Global structure and sodium ion dynamics in Mercury's magnetosphere with the offset dipole. *Journal of Geophysical Research: Space Physics*, *122*, 10,990–11,002. <https://doi.org/10.1002/2017JA024082>
- Zhang, T. L., Baumjohann, W., Du, J., Nakamura, R., Jarvinen, R., Kallio, E., et al. (2010). Hemispheric asymmetry of the magnetic field wrapping pattern in the Venusian magnetotail. *Geophysical Research Letters*, *37*, L14202. <https://doi.org/10.1029/2010GL044020>
- Zimmerman, M. I., Farrell, W. M., & Stubbs, T. J. (2013). Recursive plasma wake formation on the Moon and its effect on polar volatiles. *Icarus*, *226*(1), 992–998. <https://doi.org/10.1016/j.icarus.2013.06.013>
- Zimmerman, M. I., Jackson, T. L., Farrell, W. M., & Stubbs, T. J. (2012). Plasma wake simulations and object charging in a shadowed lunar crater during a solar storm. *Journal of Geophysical Research*, *117*, E00K03. <https://doi.org/10.1029/2012JE004094>
- Zurbuchen, T. H., Raines, J. M., Gloeckler, G., Krimigis, S. M., Slavin, J. A., Koehn, P. L., et al. (2008). MESSENGER observations of the composition of Mercury's ionized exosphere and plasma environment. *Science*, *321*(5885), 90–92. <https://doi.org/10.1126/science.1159314>
- Zurbuchen, T. H., Raines, J. M., Slavin, J. A., Gershman, D. J., Gilbert, J. A., Gloeckler, G., et al. (2011). MESSENGER observations of the spatial distribution of planetary ions near Mercury. *Science*, *333*(6051), 1862–1865. <https://doi.org/10.1126/science.1211302>